Materials Today Communications 35 (2023) 105743

Contents lists available at ScienceDirect

Materials Today Communications

journal homepage: www.elsevier.com/locate/mtcomm

Prediction of wear rates of Al-TiO_2 nanocomposites using artificial neural network modified with particle swarm optimization algorithm

Ismail Najjar [a,*], Ayman Sadoun [a], M.N. Alam [b], Adel Fathy [c,d]

[a] Mechanical Engineering Department, Faculty of Engineering, King Abdulaziz University, P.O. Box 80204, Jeddah Saudi Arabia
[b] Department of Electrical Engineering, National Institute of Technology, Warangal, India
[c] Department of Mechanical Design and Production Engineering, Faculty of Engineering, Zagazig University, P.O. Box 44519, Egypt
[d] Mechanical Department, Higher Technological Institute, Tenth of Ramadan City, Egypt

ARTICLE INFO

Keywords:
TiO_2 nanoparticle
Accumulative roll bonding
Wear behavior, ANN

ABSTRACT

The prediction of the wear rates and coefficient of friction of composite materials is relatively complex using mathematical models due to the effect of the manufacturing process on the wear properties of the composite. Therefore, this work presents a rapid reliable tool based on neural network modified with particle swarm optimizer to predict the wear rates and coefficient of friction of Al-TiO_2 nanocomposite manufactured using accumulative roll bonding (ARB). The wear rates and coefficient of the produced composites were computed using pin-on-disc and correlated with the composite morphology, hardness and microstructure. Experimentally, it was demonstrated that the hardness and wear rates reduce with increasing the number of ARB passes until a plateau was achieved due to the uniform distribution of TiO_2 nanoparticles inside the composite and the saturation of grain refinement in the Al matrix. The maximum hardness improvement was 153.7% for composite containing 3% TiO_2 nanoparticles after 5 ARB passes. While the wear rates of the same composite tested at 5 N load reduces from 3.7×10^{-3} g/m for pure Al to 1.1×10^{-3} g/m. The proposed model was able to predict the wear rates and coefficient of friction for all the produced composites tested at four different wear loads with excellent accuracy reaching R2 equal 0.9766 and 0.9866 for the wear rates and coefficient of friction, respectively.

1. Introduction

The materials we now utilize cannot keep up with the demands of ever-evolving technologies. The fact that composite materials are stronger and lighter than conventional materials like metal is one of their most distinguishing qualities. Numerous properties of composite materials, including tensile, improved impact strength, high chemical resistance, and fatigue strength, have made it possible to employ them in the building, manufacturing, aerospace, and automotive industries [1,2].

The use of composite materials with metal and ceramic matrix is increasing day by day, especially in the production of armor materials in military fields. The studies on the production of armor with new ballistic features that can resist against the ever-developing weapon systems have gained momentum recently. The high impact performance of ceramic composite materials compared to materials with monolithic structure and the use of new features have made it inevitable to be used in armor production [3–5].

One benefit of a better method for producing MMNCs is the coupling of severe plastic deformation (SPD) operations to manufacture the nanocrystalline matrix material with suitably distributed ceramic nanoparticles [6,7]. Surface composites (SCs) can be created using friction stir processing (FSP), one of the SPD techniques, without sacrificing the natural properties of the materials. However, due to asymmetric material flow during FSP, generating defect-free and evenly distributed composites in a single pass is a difficult challenge [8–10]. The capacity to form huge loads, the lack of a need for expensive equipment, and the limitless output make cumulative roll bonding (ARB) among the most promising methods [11]. The fundamental issue addressed by the ARB procedure is that edge cracks in the sheet, especially at higher strains, might develop as a result of the absence of significant hydrostatic compressive forces at the free edges [12].

Surface morphology research is a crucial component of material science that can aid in identifying and assessing physical and chemical

* Corresponding author.
E-mail address: inajjar@kau.edu.sa (I. Najjar).

https://doi.org/10.1016/j.mtcomm.2023.105743
Received 19 January 2023; Received in revised form 21 February 2023; Accepted 2 March 2023
Available online 5 March 2023

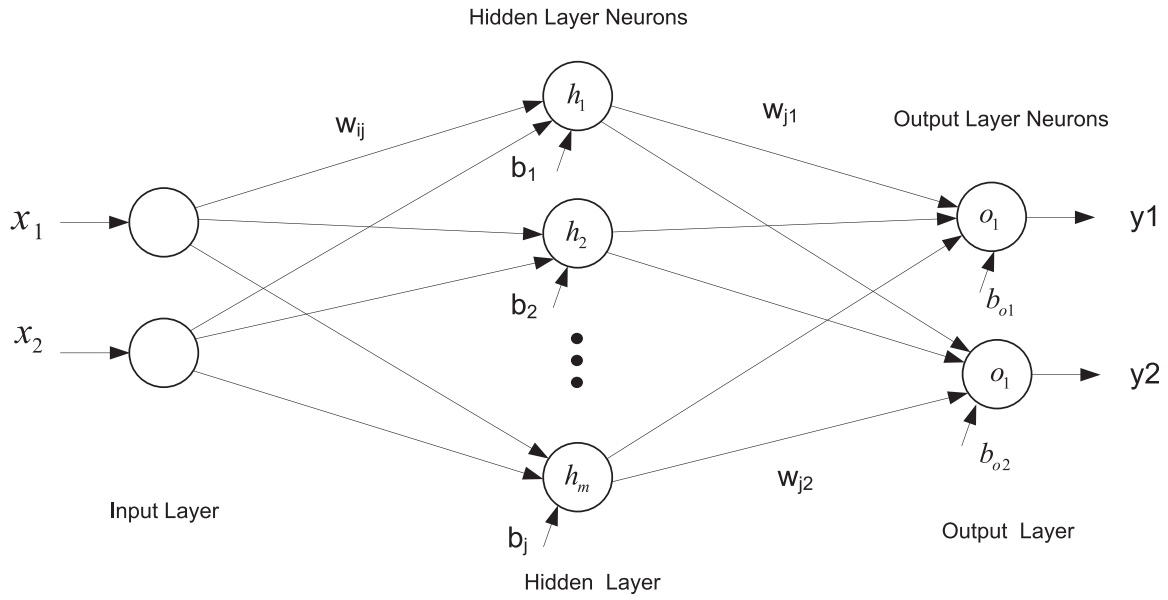

Fig. 1. ANN Structure for the considered problem.

responses such as wear, corrosion, and electrical behavior [13–15]. Utilizing ARP process for reinforcing different metals with several reinforcement particles provide a huge variety of composites with distinct properties including mechanical and electrical and wear properties [16–19]. Using the ARB method, numerous Al-based composites, such as: Al/SiC [20,21], Al/Al_2O_3 [22,23], Al/TiO_2 [24], Al/SiO_2 [25], Al/W [26], Al/WC [27–30]. The sample's significant plastic deformation during ARB is a key strengthening mechanism, which helps for grain refinement and hence increases the strength.

Wear resistance is one of the most important criteria for selecting materials especially for the materials with relative movement. The laminated sheet structures created by the ARB technique should be investigated for practical applications. ARB treated aluminum and aluminum matrix composites have been studied previously [31,32]. However, the authors reported contradicting findings, claiming that the ARB procedure increased and decreased wear resistance. In certain instances, the wear rate of ARB–processed sheets was reduced for a limited number of passes before being raised [33,34].

Recently, the applicability of machine learning in many industrial applications proved its importance as a fast and reliable prediction tool. The advantage of machine learning became more viable for problems that cannot be solved using analytical models and cannot be simply governed using mathematical formulations. This increases the applicability of machine learning models in composite fields where complex phenomenon could occur during manufacturing [35,36]. Some recent works applied different machine learning models to predict the wear rates of copper based composites, that showed good predictability of the wear rates [37,38]. Also, it was used to predict different mechanical and chemical properties of composites [39–44]. However, most of the deployed model for prediction of mechanical and wear properties of composite materials, consider complex machine learning model such as long-short term memory model and dendritic neural and deep neural networks, which require complex implementation and computation cost [45].

Therefore, this work presents a simple model that uses conventional neural network modified with particle swarm optimization algorithm to fast and reliably predict the wear rates and coefficient of friction of Al-TiO_2 nanocomposites developed in this work. The Al-TiO_2 nanocomposites was manufactured using ARB technique at different passes. The microstructural and morphology changes during the ARB process were evaluated to optimize the microstructure of the composite. The wear rates and coefficient of friction were evaluated using pin-on-disc experiment and correlated with the material microstructure and the hardness. Finally, the developed artificial neural network modified with particle swarm optimization algorithm was employed to predict the wear rates and coefficient of friction.

2. Modeling

2.1. Artificial neural network

It has a great potential to tune weights and biases of the ANN model of any size. In the proposed work, the PSO algorithm is devised to tune a generalized feed-forward Ann model considering multi neurons in the hidden layer. The developed model is shown in the Fig. 1. Here, the weight and biases of the network are represented by the position vector of PSO. Thus, each particle represents a set of weights and biases of the developed ANN model of the problem considered in this paper. After solving the problem, the final weights and biases are obtained of the feed-forward network that is well trained with the potential to predict outputs of any unknown features.

Let us try to discuss the working principle of ANN in details with the help of Fig. 1. The ANN model has a hidden layer of m neurons and the output layer with two neurons. The input layer can receive dataset 2 data points in each input sample. In other words, this ANN structure is for relating 2 independent variables to two single output or dependent variable. Mathematically, it can be represented as:

$$[y1, y2] = f(x_1, x_2, w, b) \tag{1}$$

Where x_1 and x_2 are independent variables of a given sample and y1 and y2 are the outputs dependent on them. Here, **w** and **b**are weight and bias matrices of the ANN structure. In ANN, this relationship is represented using a very complex mathematical equation based on the activation function considered for each neuron. Normally, the same activation function is considered for all the neurons of each layer of the network. The activation function is also called a transfer function. Commonly, Linearized transfer function is used in output layer whereas sigmoid or hyperbolic tangent function is used in the hidden layer.

The output of a neuron is calculated based on the inputs, weights and bias of the network. The relationship between them is expressed with the help of the considered transfer function. Mathematically, the input and output of a neuron is expressed as:

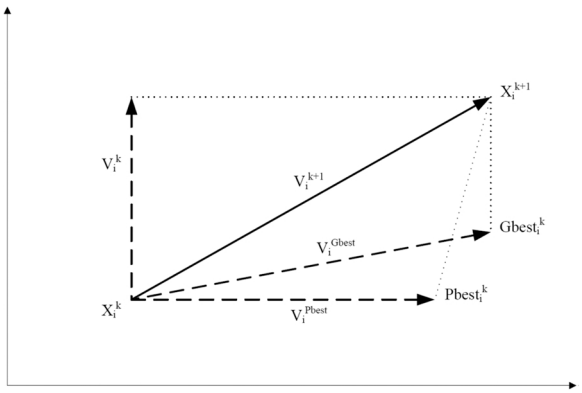

Fig. 2. PSO Search Mechanism.

$$z = g\left(b + \sum_{i=1}^{n} w_i x_i\right) \tag{2}$$

Where *g*is the activation or transfer function of neuron. Through training with the known values of inputs (x_1, x_2) and their corresponding outputs (y1, y2), the weight matrix **w** and bias matrix **b** are updated. When a large number of input vectors and output vectors are used in the training, the optimal values of **w** and **b** are obtained. Once training is completed the ANN model gets ready for giving output for any unknown input vector (x_1, x_2). Training is not an easy task. Here, various algorithms are used to obtain the optimum values of **w** and **b** so that least possible error is obtained in the training phase. This problem can be formulated as an optimization problem where objective function is minimization of error square in target and the predicted output subject to keeping weight and bias values within a fixed boundary. In this paper, PSO algorithm is utilized to get the optimum values of **w** and **b** of ANN model whose details are discussed subsequently.

2.2. Particle swarm optimization algorithm

Particle swarm optimization is a promising method for solving complicated optimization problems in most areas. This method is inspired by swarm intelligence displayed by fish schooling and birds flocking. Mathematical, the method is guided primarily by two equations associated with velocity and positive updates of the swarm. To get mathematical aspects of PSO, let us assume a matrix **X** and **V**, representing the swarm position and velocity of PSO in multi-dimensional search space. Here, **X** and **V** can be expressed as follows;

$$\boldsymbol{X} = \left[x_{ij}\right] for i = 1, 2, ..., m; i = 1, 2, ..., n \tag{3}$$

$$\boldsymbol{V} = \left[V_{ij}\right] for i = 1, 2, ..., m; i = 1, 2, ..., n \tag{4}$$

Each row of **X** represents a particle whose velocity is represented by the corresponding row of **V** in this m-dimensional search space having the total number of particles n in the PSO algorithm. As the algorithm iteration continues, the position and velocity of each particle and the whole swarm are updated. This change always targets moving towards the global optimal position where particles achieve their goals. In other words, with fish schooling and birds flocking, the objective of getting their food is achieved. Mathematically, position update of each particle is dependent on three main components. These components are their position, their personal memory-based best position and the whole swarm memory-based position. Also, the next position is closely associated with the velocity of each particle in each of the directions of the components mentioned above. Thus, the velocity update of each particle decides its next position. Fig. 2 shown the search mechanism in PSO algorithm.

The velocity update of a particle is defined as

$$V_{ij}^{k+1} = V_{ij}^{k} + c_1 r_1 \left(Pbest_{ij}^{k} - X_{ij}^{k}\right) + c_2 r_2 \left(Gbest_{j}^{k} - X_{ij}^{k}\right) \tag{5}$$

In the above equation, the first term is associated with the inertia of the particle, the second term is associated with the personal memory of the particle, and the third term is associated with the overall best memory of the swarm. These factors give a new direction vector for the particle to move accordingly. Here, c_1 and c_2 are called acceleration factors of PSO associated to personal best and global best terms, while r_1 and r_2 are two randomly generator numbers in [− 1,1]. The next position of the particle is defined using the updated velocity as follows.

$$X^{k+1} = X_{ij}^{k} + V_{ij}^{k+1} \tag{6}$$

Once the new position and all particles, i.e., the swarm, are obtained, personal memory and overall swarm or global memory of the swarm are updated. The personal and global best is the position of the particle and the swarm, which was the best until the current iteration. To update **Pbest** and **Gbest** at each iteration, the fitness function is evaluated using the position of each particle. In reality, each particle represents a solution vector that can solve an optimization problem by satisfying its constraints. The fitness function represents the entire constrained optimization problem whose value needs to be evaluated, and **Pbest** and **Gbest** are updated using the following logic.

$$Iff\left(X_i^{k+1}\right) < f\left(Pbest_i^{k}\right) \text{then} Pbest_i^{k+1} = X_i^{k+1} \text{else} Pbest_i^{k+1} = Pbest_i^{k}; \tag{7}$$

$$Iff\left(X_i^{k+1}\right) < f\left(Gbest^{k}\right) \text{then} Gbest^{k+1} = X_i^{k+1} \text{else} Gbest^{k+1} = Gbest^{k}; \tag{8}$$

It is to be noted that **Pbest** is related to each particle, whereas **Gbest** is related to the swarm. The best is the same for each, while **Pbest** is different.

After this, stopping criteria are checked and repeated from upgrading the position vector of each particle until the global optimal solution is achieved or stopping criteria are met. Usually, a predefined number of iterations is set as the stopping criteria. Also, when the solution does not improve for a subsequent fixed number of iterations, then the algorithm is stopped. A combination of these two stopping criteria works well and is usually adopted as is considered in this work.

2.3. Training ANN Model using PSO

The network needs to be trained after the ANN's structure has been established. Finding the ideal values for the network's weights and biases is the process of training the network. Finding the appropriate weights and biases for the ANN often involves using a variety of strategies. In this work, PSO algorithm has been used to train the network. Here, the training problem is defined as an optimization problem with the objective to minimize the mean square error subject to keeping the values of weights and biases within a range of [− 1.5, 1.5]. This range can be different and be easily modified in the developed programs.

Here, weights and biases of considered ANN model is used to form a vector called particle for PSO. Collection of many such particles forms a swarm of PSO. Hence, any particle gives weights and biases of the ANN model which once assigned to it, gives a prediction for any given set of input. To obtain the optimum values of weights and biases, PSO is applied on this randomly initialized swarm and optimal swarm is obtained. The **Gbest** of this optimized swarm gives the optimized values weights and biases which are used in the ANN model to form it ready for prediction.

Mathematically, this problem is formulated as:

$$OF = \min \sum_{i=1}^{N} \left(target(i) - output(i)\right)^2 \tag{9}$$

Subject to

$$w_{\min} \le w_{ij}^{l} \le w_{\max}$$

Table 1
Chemical composition of used Al1100 sheets.

Elements	Zn	Mg	Cu	Mn	Si	Fe	Ti	V	Al
wt%	**0.05**	**0.05**	**0.05**	**0.05**	**0.25**	**0.4**	**0.03**	**0.05**	**Balance**

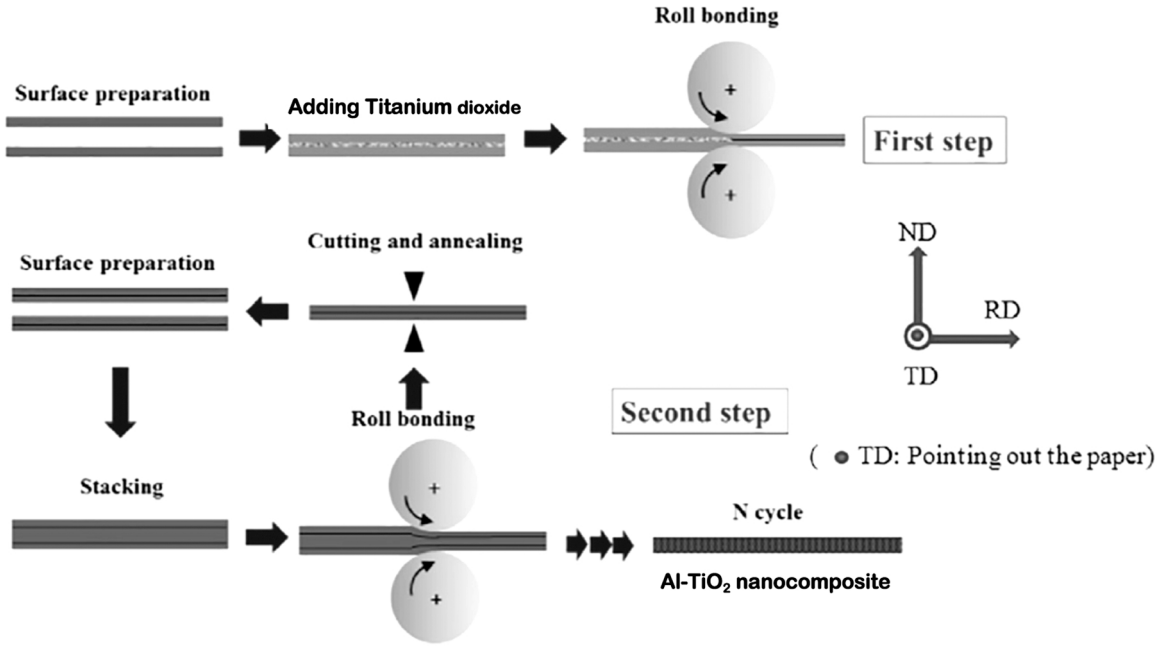

Fig. 3. Schematic illustration of ARB process.

$$b_{\min} \le b_j^l \le b_{\max}$$

Where $target(i)$ is the know target value of a given input sample i while $output(i)$ is the output value of the ANN model when this given input sample i is passed through the ANN model. Here, the main task is to find out the values of weights and biases of the network in such a way that objective function $OF$is minimized.

2.4. Prediction of wear rates and coefficient of friction using ANN-PSO model

The ANN-PSO model developed in this work was used to predict the wear rates of the Al-TiO_2 nanocomposite that was prepared and characterized as detailed in the next section. The input to the model was the number of rolling pass and the wear load. While the output was the wear rates and coefficient of friction. The typical ANN model was used as well to predict the wear rates and coefficient of friction. The accuracy of the developed model was compared with typical ANN model and evaluated using three measures, namely determination coefficient (R^2), root mean square error (RMSE), and Mean absolute error (MAE) as:

$$R^2 = \frac{\left(\sum_{i=1}^{m_s}(h_i-\overline{h})(k_i-\overline{k})\right)^2}{\sum_{i=1}^{m_s}(h_i-\overline{h})^2 \times \sum_{i=1}^{m_s}(k_i-\overline{k})^2} \quad (10)$$

$$RMSE = \sqrt{\frac{1}{m_s}\sum_{i=1}^{m_s}(h_i-k_i)^2} \quad (11)$$

$$MAE = \frac{1}{m_s}\sum_{i=1}^{m_s}|h_i-k_i| \quad (12)$$

where m_s, h, and k are the number of experimental datasets, experimental value and the computed value, respectively. While $\overline{h}$ and $\overline{k}$ are the mean values of the experimental and computed data, respectively.

3. Materials and methods

3.1. Materials and samples preparation

The matrix of the composite was made entirely of commercial Al 1100. Table 1 provides the chemical make-up of the Al matrix. In order to enhance the mechanical and surface qualities of the Al sheets, they were heated to 275 degrees in a thermal furnace for over an hour before being cooled to room temperature (the annealing process). The TiO_2 nanoparticle powder reinforcement phase had particles that were, on average, 70 nm in size. The creation of Al-TiO_2 composites using the ARB method is shown in Fig. 3. To create rough surfaces, both sides of aluminum sheets were wire brushed with wire having a diameter of 0.3 mm after being degreased with acetone to remove surface impurities. The TiO_2 nanoparticles were ultrasonically sonicated in acetone for 90 s to prevent clustering/agglomerations. The cluster-free particles were then sprayed uniformly on the scratch-brushed sheets' surface using a gas atomizer. The composites had TiO_2 nanoparticle concentrations ranging from 0 to 3 wt%, with a 1% step. In the first rolling pass, the cross-section was reduced by 60%, and in succeeding passes, by 50%. The middle of the rolled samples was then removed. Only the first pass of each rolling process, which might happen up to five times, involved continually introducing TiO_2 powders.

3.2. Microscopic observations

The edges of the rolled sheets were cut and the samples were cut from the central part in normal direction (RD - ND planes), then used SiC emery sheets of varying grits and Keller's reagent to polish and etch.

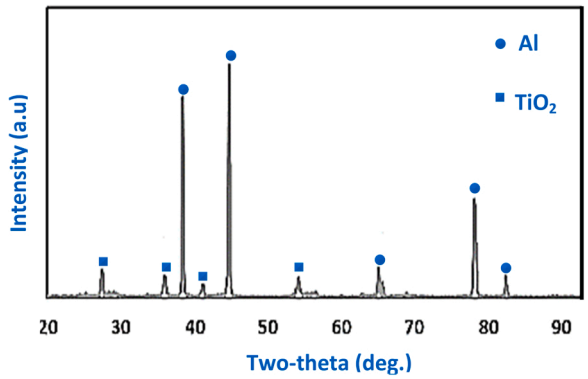

Fig. 4. XRD of the Al – 3% TiO_2 nanocomposite sheets after 5 ARB passes.

Layer morphology and thickness of the samples were examined in an FEI Quanta scanning electron microscope (SEM) equipped with an energy-dispersive X-ray spectrometer (EDS). In order to show how the TiO_2 nanoparticles dispersed and how the Al sheets adhered to one another, scanning electron microscopy (SEM) and energy dispersive spectroscopy (EDS) studies in the cross section of the rolled sheets were conducted.

3.3. Hardness and wear evaluations

A micro-Vickers device was used for the Vickers test, which was carried out in accordance with ASTM-E384 standard, and a load of 0.1 kg was applied for 20 s. For each specimen, the hardness was assessed at five randomly chosen sites, and the average values were used to calculate the microhardness of the sample. Utilizing a pin-on-disk wear apparatus, the wear behavior of the generated composites was evaluated. 120 mm length by 20 mm wide rectangular samples were the ones we used. Between two surfaces that were in touch, there was a linear velocity of 1 m/s. For a sliding distance of 200 m, each wear test was conducted three times. Wear tests were done with typical loads of 5, 10, 15, and 20 N to look at how normal load affected wear rate. SEM analysis was used to identify the worn surface and examine wear track features.

4. Results and discussion

4.1. Microstructural observation

Fig. 4 shows the XRD analysis of Al-3%TiO_2 nanocomposite production after 5 passes. Only two phases were observed for TiO_2 and Al phases. The presence of only these two phases demonstrate the purity of the produced composite and it was free of any intermetallic and impurities.

In Fig. 5, SEM images of Al-TiO_2 nanocomposites with various reinforcement contents are displayed. There were three layers of TiO_2 nanoparticles sandwiched between four Al sheets. Ceramic nanoparticles may first collect in the aluminum matrix in clusters. This tendency intensifies with the addition of reinforcement. After the initial pass, the matrix-reinforcement relationship would become weak, resulting in uneven reinforcement dispersal between matrixes.

Particle clumping is decreased by using more passes. In Fig. 5c, the cross section of the composite made of Al and 3% TiO_2 is displayed, which shows how the particles cluster less. With several passes, there is a reduction in the distance between the sheet interfaces. When adjacent metal surfaces are heated and rolled afterward, interatomic diffusion (atom-to-atom bonding) takes place, improving adhesion (bond strength) between them [46,47]. Finally, as seen in Fig. 5c and d, rolling after annealing resulted in the contact becoming tightly bound, making it challenging to find the interface even with SEM analysis.

4.2. Hardness

Fig. 6 shows the microhardness evolution and the improvement rates

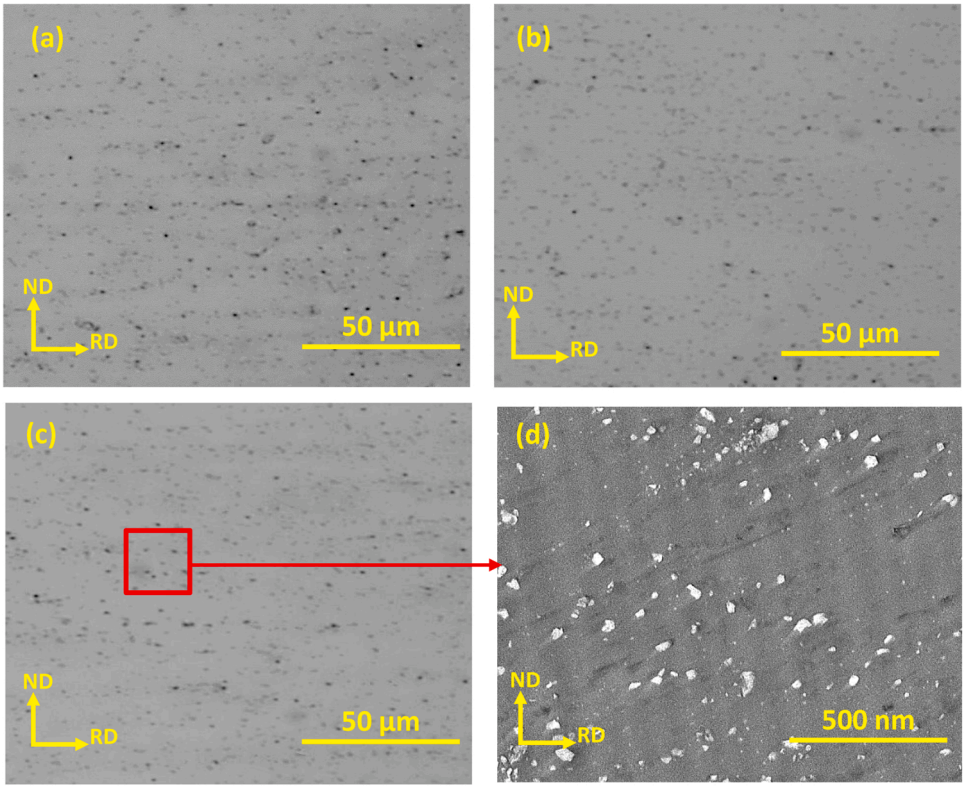

Fig. 5. SEM micrograph ofAl - TiO_2 nanocomposite sheets after 5 ARB passes: (a) 1%, (b) 2%, (c) 3%, (d) larger magnification for sample with 3% TiO_2.

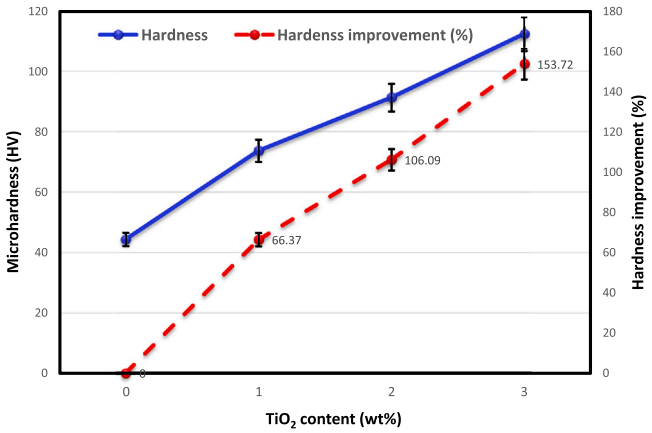

Fig. 6. Microhardness ofAl - TiO_2 nanocomposite sheets after 5 ARB passes.

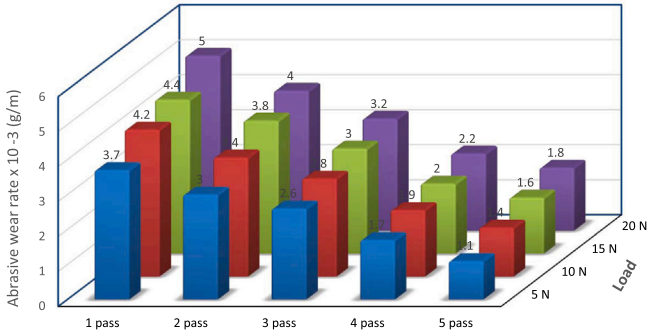

Fig. 7. Variations of abrasive wear rate versus number of passes for ARB-processed Al–3% TiO_2 nanocomposite samples in the different applied load.

for Al-TiO_2 nanocomposites with different TiO_2 content after 5 passes. The hardness of all the produced composites were greater than the pure Al. The Al-3%TiO_2 nanocomposite had the highest hardness value. The existence of a hard phase in the nanocomposite and the addition of TiO_2 to the Al matrix both improved hardness as a result of the pore-closing mechanism. Due to the increase in tensile strength in the fifth pass, the microhardness in the fifth pass relative to other samples increased suddenly. The findings of this experiment have been previously published [48,49], and in general, the hardness of aluminum has grown following accumulative rolling bonding. A nanocomposites made of Al-3 wt% TiO_2 have a hardness value of 116 HV compared to pure aluminum's 44 HV. Scratch brushing, cold working, grain refining, and the addition of TiO_2 nanoparticles were all credited with this significant rise. Additionally, Al-3 wt% TiO_2 nanocomposites' hardness was much higher than that of the other two composites, Al-1 wt% TiO_2 and Al-2 wt % TiO_2, with improvement percentages of 53% and 153%, respectively. This novel method significantly improves ARB by combining good interfacial bonding between Al and TiO_2 with a homogenous dispersion of TiO_2 nanoparticles within the Al matrix. The improvement was brought about by the consistent dispersion of TiO_2 nanoparticles between the sheets, where there is little chance of agglomeration during up to five cycles of rolling (see Fig. 6). On the other hand, strain hardening and dislocation effects were produced as a result of dislocation density and locked to stop dislocations [50]. The greatest improvement attained in [51] is 68%, but the improvement rate for Al-TiO_2 composites reaches 153% for composite with 3% reinforcement in both situations. As a comparison reinforcement phase, SiO_2 has a substantially lower improvement rate than Al-TiO_2 composites.

4.3. Wear behavior and ANN-PSO prediction

The wear rate of an Al-3 wt% TiO_2 nanocomposite treated for several ARB passes is depicted in Fig. 7. As the number of ARB passes increased for all the applied loads, the wear rates decreased. The material's hardness and strength are increased during the ARB process, resulting in a decreased wear rate for ARBed Al. As a result, there are fewer plastic deformations at the contact surface, which leads to less material removal and lower wear rates. As a result, sample wear resistance gets better as the number of ARB passes rises. The physical and mechanical characteristics of the material affect the rate of wear [52–54]. This chart shows that when the usual load increases, the wear rate of each sample under examination also increases. This is because the pin penetrated the sample more deeply, which causes larger rates of material removal. Similar to the indentation experiment, where the depth of the indentation grows as the applied load decreases, the effect of the wear load causes an increase in the indentation [55,56]. It was noted that the wear rate was proportional to the normal applied load for Al-3 wt% TiO_2 nanocomposite processed for different ARB passes, as stated by Archard's law. In other words, uniform TiO_2 nanoparticle distribution reduces wear rate. This is owing to the Al matrix's work hardening effect and the TiO_2 nanoparticles' dislocation strengthening mechanism. Additionally, higher passes result in lower porosities between TiO_2 nanoparticles and the aluminum base matrix, which increases bonding strength and reduces wear rate [57].

Fig. 8 shows the surface morphology of the worn surfaces of pure Al and Al-3 wt% TiO_2 nanocomposite after five ARB passes. A comprehensive investigation revealed the usual characteristics of abrasive wear, such as abrasion grooves generated in the sliding direction and ploughing, for beginning aluminum. A large quantity of fine agglomerated wear particles primarily filled the grooves on the worn surface. The wear mechanism changes as the ARB passes and the layer count increases; delamination wear occurs, and coarse flakes form with fine particles. The delamination wear characteristics of the sample ARB-processed by 5 passes were attributed to fracture by crack propagation in the interlayer sub-worn surface. Finally, when compared to

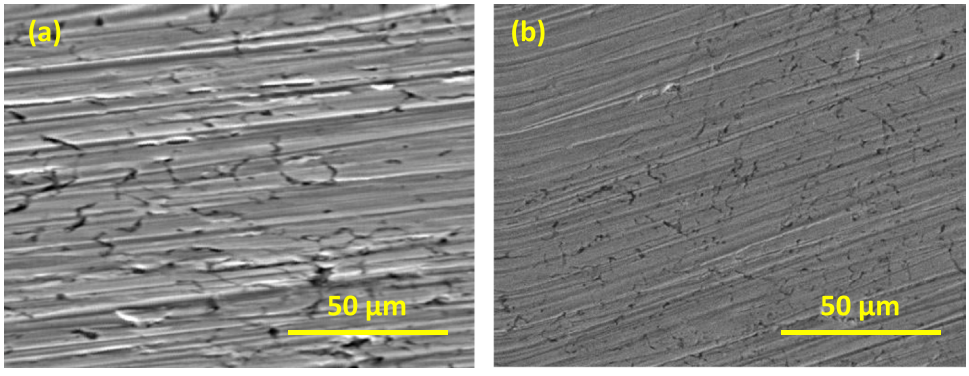

Fig. 8. SEM images of worn surface of (a) Al/Al and (b) Al–3%TiO_2.

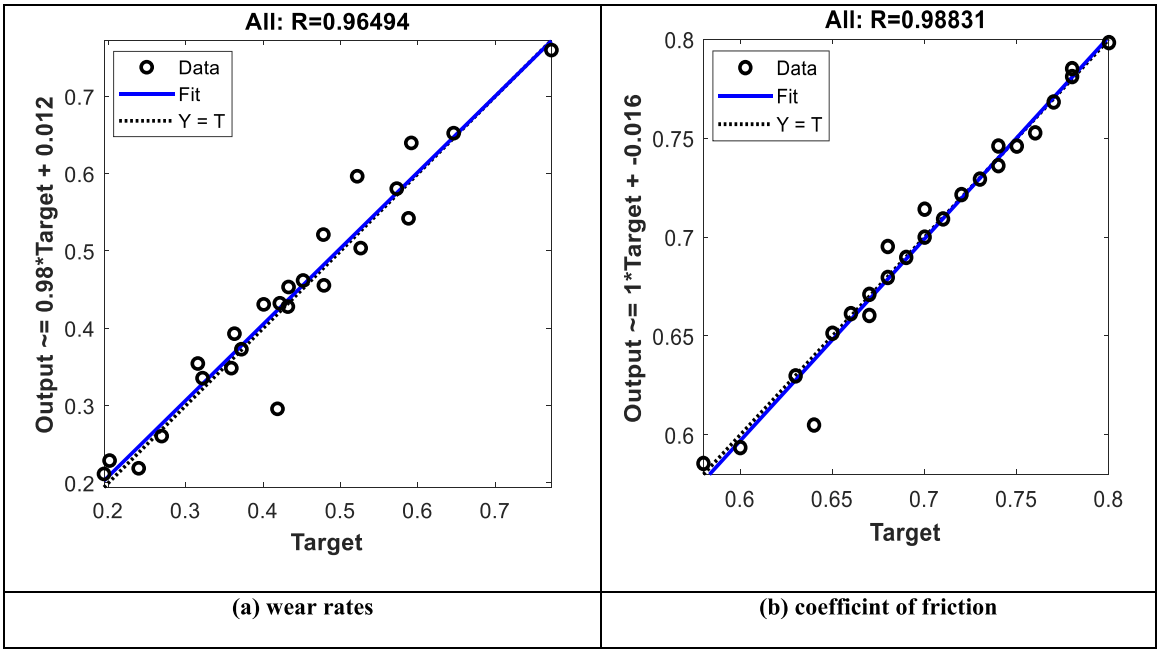

Fig. 9. Prediction of ANN model for the wear rates and coefficient of friction.

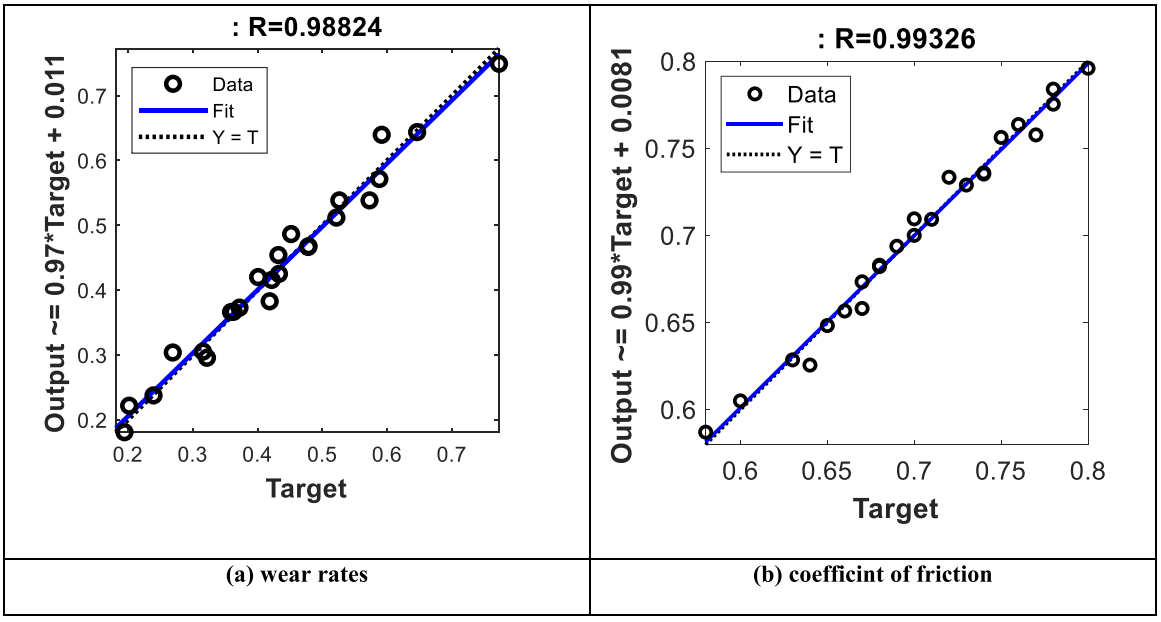

Fig. 10. Prediction of ANN-PSO model for the wear rates and coefficient of friction.

monolithic samples, composite samples supplemented with 3 wt% TiO_2 nanoparticles exhibit greater wear resistance. Based on the foregoing considerations, high temperature caused grain formation at the plastically deformed region (between the pin and the worn surface) following the start of wear. Because of local work hardening of the aluminum matrix around the particles, increasing the percent TiO_2 reduces the width of wear grooves and enhances wear resistance.

Fig. 9 shows the perdition of the typical ANN model for the wear rates and coefficient of friction at different wear loads and number of passes for Al-TiO_2 nanocomposites. As shown in the figure, the ANN model prediction deviates from the experimental results significantly, especially at larger wear rates which was obtained at high wear loads. The deviation is some of the data reaches more than 20%, which is relatively large when considering the accuracy required for such materials and their applications. However, the prediction of ANN model is better for the coefficient of friction with maximum deviation of 8%.

Fig. 10 shows the prediction of ANN-PSO model for the wear rates and the coefficient of friction of the same material. As observed in the figure, perfect prediction of both wear rates and coefficient of friction

Table 2
Accuracy of the ANN-PSO model.

Particulars	Output 1	Output 2
R-square	0.9766	0.9866
RMSE	0.0213	0.0066
MAE	0.0172	0.0052
SD	0.1405	0.0580

was obtained using the ANN-PSO model. The accuracy of the model was confirmed with the R2, RMSE, and MAE for the model prediction, which showed 0.9766,.0213, and 0.0172 for the wear rates and 0.9866,.0066, and 0.0052 for the coefficient of friction, Table 2. Standard deviation (SD) of the output corresponding to wear rates and coefficient of friction is 0.1405 and 0.0580 respectively as can be observed from Table 2.

5. Conclusions

This paper presents experimental and machine learning prediction of wear rates of Al-TiO_2 nanocomposite with different TiO_2 content produced by accumulative roll bonding technique. The wear properties of the produced composites were evaluated using pin-on-disc experiment and correlated with the morphology, microstructure, and hardness. A machine learning model was developed based on neural network and particle swarm optimization algorithm to predict the wear rates and coefficient of friction. Based on the result obtained the following conclusions can be drawn:

- Al-3 wt% TiO_2 nanocomposites hardness reached 114 HV which was much higher than that of pure Al achieving 153.7% improvement. This composite showed higher hardness compared to the composites reinforced with 1 and 2 wt% of TiO_2 nanoparticles.
- The wear rate reduced significantly with increasing the number of ARB passes reaching 1.1×10^{-3} g/m for Al-3 wt% TiO_2 nanocomposites compared to 3.7×10^{-3} g/m for pure Al due to the grain refinement mechanisms and hardness increase.
- The wear rates increases with increasing the wear load for at all considered passes due to the larger contact are between the pin and the disc, which increases plastic deformation during testing and the material removal rate.
- The developed model predicted the wear rates and coefficient of friction much better than the conventional neural network. The accuracy of the developed model for prediction reaching R2 values of 0.9766 and 0.9866 respectively.

Declaration of Competing Interest

The authors declare that they have no known competing financial interests or personal relationships that could have appeared to influence the work reported in this paper.

Data Availability

No data was used for the research described in the article.

Acknowledgement

The authors extend their appreciation to the Deputyship for Research & Innovation, Ministry of Education in Saudi Arabia for funding this research work through the project number (IFPIP- 41-135-1443) and King Abdulaziz University, DSR, Jeddah, Saudi Arabia.

References

[1] D. Rahmatabadi, B. Mohammadi, R. Hashemi, T. Shojaee, An experimental study of fracture toughness for nano/ultrafine grained Al5052/Cu multilayered composite processed by accumulative roll bonding, J. Manuf. Sci. Eng. 140 (10) (2018).
[2] A.M. Sadoun, I.M.R. Najjar, M.S. Abd-Elwahed, A. Meselhy, Experimental study on properties of Al–Al2O3 nanocomposite hybridized by graphene nanosheets, J. Mater. Res. Technol. 9 (6) (2020) 14708–14717.
[3] H. Ahmadian, A.M. Sadoun, A. Fathy, T. Zhou, Utilizing a unified conceptual dynamic model for prediction of particle size of duel-matrix nanocomposites during mechanical alloying, Powder Technol. (2023), 118291.
[4] M. Malaki, A.F. Tehrani, B. Niroumand, Fatigue behavior of metal matrix nanocomposites, Ceram. Int. 46 (15) (2020) 23326–23336.
[5] R. Taherzadeh Mousavian, S. Behnamfard, A. Heidarzadeh, K. Taherkhani, R. Azari Khosroshahi, D. Brabazon, Incorporation of SiC ceramic nanoparticles into the aluminum matrix by a novel method: production of a metal matrix composite, Met. Mater. Int. 27 (8) (2021) 2968–2976.
[6] A.M. Sadoun, F. Abd El-Wadoud, A. Fathy, A.M. Kabeel, A.A. Megahed, Effect of through-the-thickness position of aluminum wire mesh on the mechanical properties of GFRP/Al hybrid composites, J. Mater. Res. Technol. 15 (2021) 500–510.
[7] A.M. Sadoun, A.F. Meselhy, A.W. Deabs, Improved strength and ductility of friction stir tailor-welded blanks of base metal AA2024 reinforced with interlayer strip of AA7075, Results Phys. 16 (2020), 102911.
[8] S. Rathee, S. Maheshwari, A.N. Siddiquee, M. Srivastava, Distribution of reinforcement particles in surface composite fabrication via friction stir processing: suitable strategy, Mater. Manuf. Process. 33 (3) (2018) 262–269.
[9] S. Rathee, S. Maheshwari, A.N. Siddiquee, M. Srivastava, A review of recent progress in solid state fabrication of composites and functionally graded systems via friction stir processing, Crit. Rev. Solid State Mater. Sci. 43 (4) (2018) 334–366.
[10] G.S. Alsoruji, A.M. Sadoun, M. Abd Elaziz, M.A. Al-Betar, A.W. Abdallah, A. Fathy, On the prediction of the mechanical properties of ultrafine grain Al-TiO2 nanocomposites using a modified long-short term memory model with beluga whale optimizer, J. Mater. Res. Technol. (2023).
[11] N. Tsuji, Y. Saito, S.H. Lee, Y. Minamino, ARB (Accumulative Roll-Bonding) and other new techniques to produce bulk ultrafine grained materials, Adv. Eng. Mater. 5 (5) (2003) 338–344.
[12] Y. Saito, H. Utsunomiya, N. Tsuji, T. Sakai, Novel ultra-high straining process for bulk materials—development of the accumulative roll-bonding (ARB) process, Acta Mater. 47 (2) (1999) 579–583.
[13] A. Hassan, A. El-Hamid, A. Wagih, A. Fathy, Effect of mechanical milling on the morphologyand structural evaluation of Al-Al2O3 nanocomposite powders, Int. J. Eng. 27 (4) (2014) 625–632.
[14] N.E. Mahallawy, A. Fathy, M. Hassan, W. Abdelaziem, Evaluation of mechanical properties and microstructure of Al/Al–12% Si multilayer via warm accumulative roll bonding process, J. Compos. Mater. (2017), 0021998317692141.
[15] D. Rahmatabadi, M. Pahlavani, M.D. Gholami, J. Marzbanrad, R. Hashemi, Production of Al/Mg-Li composite by the accumulative roll bonding process, J. Mater. Res. Technol. 9 (4) (2020) 7880–7886.
[16] X. Rao, Y. Wu, X. Pei, Y. Jing, L. Luo, Y. Liu, J. Lu, Influence of rolling temperature on microstructural evolution and mechanical behavior of AZ31 alloy with accumulative roll bonding, Mater. Sci. Eng.: A 754 (2019) 112–120.
[17] M. El-wazery, A. Fathy, Electrical and mechanical performance of zirconia-nickel functionally graded materials, Int. J. Eng. 26 (4) (2013) 375–382.
[18] K.V. Ivanov, V.E. Ovcharenko, Structural features of ultrafine-grained aluminum processed through accumulative roll bonding providing improved mechanical properties and thermal stability, Mater. Sci. Eng.: A 775 (2020), 138988.
[19] A.M. Sadoun, A. Wagih, A. Fathy, A.R.S. Essa, Effect of tool pin side area ratio on temperature distribution in friction stir welding, Results Phys. 15 (2019), 102814.
[20] A. Fathy, D. Ibrahim, O. Elkady, M. Hassan, Evaluation of mechanical properties of 1050-Al reinforced with SiC particles via accumulative roll bonding process, J. Compos. Mater. 53 (2) (2019) 209–218.
[21] A.F. Meselhy, M.M. Reda, Investigation of mechanical properties of nanostructured Al-SiC composite manufactured by accumulative roll bonding, J. Compos. Mater. 53 (28–30) (2019) 3951–3961.
[22] A. Mohamed, M.M. Mohammed, A.F. Ibrahim, O.A. El-Kady, Effect of nano Al2O3 coated Ag reinforced Cu matrix nanocomposites on mechanical and tribological behavior synthesis by P/M technique, J. Compos. Mater. 54 (30) (2020) 4921–4928.
[23] A. Wagih, A. Fathy, T.A. Sebaey, Experimental investigation on the compressibility of Al/Al2O3 nanocomposites, Int. J. Mater. Prod. Technol. 52 (3–4) (2016) 312–332.
[24] I.R. Najjar, M. Elmahdy, Study of mechanical properties and wear resistance of nanostructured Al 1100/TiO2 nanocomposite processed by accumulative roll bonding, J. Compos. Mater. (2022), 00219983221103636.
[25] A. Fathy, A. Shaker, M.A. Hamid, A.A. Megahed, The effects of nano-silica/nano-alumina on fatigue behavior of glass fiber-reinforced epoxy composites, J. Compos. Mater. 51 (12) (2017) 1667–1679.
[26] S. Amirkhanlou, M. Ketabchia, N. Parvin, Sh Khorsand, R. Bahrami, Accumulative Press Bonding; a novel manufacturing process of nanostructured metal matrix composites, Mater. Des. 51 (2013) 367–374.
[27] C.Y. Liu, Q. Wang, Y.Z. Jia, B. Zhang, R. Jing, M.Z. Ma, Q. Jing, R.P. Liu, Effect of W particles on the properties of accumulatively roll bonded Al/W composites, Mater. Sci. Eng.: A 547 (2012) 120–124.
[28] B. Azad, E. Borhani, H.M. Semnani, Fracture behavior of Al-0.2 wt% Zr alloy processed by accumulative roll-bonding (ARB) process, Kov. Mater. 54 (1) (2016) 9–15.
[29] B. Azad, H.M. Semnani, E. Borhani, Microstructure evolution and mechanical properties of nano-structured Al–0.2 wt% Zr alloy fabricated by Accumulative Roll Bonding (ARB) process, Trans. Indian Inst. Met. 70 (10) (2017) 2725–2732.
[30] M. Elwan, A. Fathy, A. Wagih, A.R.S. Essa, A. Abu-Oqail, A.E. EL-Nikhaily, Fabrication and investigation on the properties of ilmenite (FeTiO3)-based Al composite by accumulative roll bonding, J. Compos. Mater. 54 (10) (2020) 1259–1271.
[31] S. Khatir, D. Boutchicha, C. Le Thanh, H. Tran-Ngoc, T.N. Nguyen, M. Abdel-Wahab, Improved ANN technique combined with Jaya algorithm for crack identification in plates using XIGA and experimental analysis, Theor. Appl. Fract. Mech. 107 (2020), 102554.
[32] R. Zenzen, S. Khatir, I. Belaidi, C. Le Thanh, M.A. Wahab, A modified transmissibility indicator and Artificial Neural Network for damage identification

and quantification in laminated composite structures, Compos. Struct. 248 (2020), 112497.
[33] S. Wang, H. Wang, Y. Zhou, J. Liu, P. Dai, X. Du, M.A. Wahab, Automatic laser profile recognition and fast tracking for structured light measurement using deep learning and template matching, Measurement 169 (2021), 108362.
[34] W. Zhao, L. Wang, S. Mirjalili, Artificial hummingbird algorithm: a new bio-inspired optimizer with its engineering applications, Comput. Methods Appl. Mech. Eng. 388 (2021), 114194.
[35] N. Hasheminejad, G. Pipintakos, C. Vuye, T. De Kerf, T. Ghalandari, J. Blom, W.V. D. Bergh, Utilizing deep learning and advanced image processing techniques to investigate the microstructure of a waxy bitumen, Constr. Build. Mater. 313 (2021), 125481.
[36] A. Sadoun, I. Najjar, A. Fathy, M.A. Elaziz, M.A. Al-Qaness, A. Abdallah, M. Elmahdy, An enhanced Dendritic Neural Algorithm to predict the wear behavior of alumina coated silver reinforced copper nanocomposites, Alex. Eng. J. (2022).
[37] M.R. Dobbelaere, P.P. Plehiers, R. Van de Vijver, C.V. Stevens, K.M. Van Geem, Machine learning in chemical engineering: strengths, weaknesses, opportunities, and threats, Engineering 7 (2021) 1201–1211.
[38] S. Zhong, K. Zhang, M. Bagheri, J.G. Burken, A. Gu, B. Li, X. Ma, B.L. Marrone, Z. J. Ren, J. Schrier, et al., Machine learning: new ideas and tools in en-vironmental science and engineering, Environ. Sci. Technol. 55 (2021) 12741–12754.
[39] A.M. Sadoun, I.R. Najjar, G.S. Alsoruji, A. Wagih, M.A. Elaziz, Utilizing a long short-term memory algorithm modified by dwarf mongoose optimization to predict thermal expansion of Cu-Al2O3 nanocomposites, Mathematics 10 (2022) 1050.
[40] I. Najjar, A. Sadoun, G.S. Alsoruji, M.A. Elaziz, A. Wagih, Predicting the mechanical properties of Cu–Al2O3 nanocomposites using machine learning and finite element simulation of indentation experiments, Ceram. Int. 48 (2022) 7748–7758.
[41] A.M.A. Haimed, T. Saba, A. Albasha, A. Rehman, M. Kolivand, Viral reverse engineering using Artificial Intel-ligence and big data COVID-19 infection with Long Short-term Memory (LSTM), Environ. Technol. Innov. 22 (2021), 101531.
[42] J.K. Khabushan, S.B. Bonabi, Investigating of the microstructure and mechanical properties of Al-based composite reinforced with nano-trioxide tungsten via accumulative roll bonding process, Open J. Met. 7 (1) (2017) 9–23.
[43] D. Saber, K. Abd El-Aziz, A. Fathy, Corrosion behavior of copper–alumina nanocomposites in different corrosive media, Int. J. Mech. Eng. 5 (2016) 1–10.
[44] D. Rahmatabadi, A. Shahmirzaloo, M. Farahani, M. Tayyebi, R. Hashemi, Characterizing the elastic and plastic properties of the multilayered Al/Brass composite produced by ARB using DIC, Mater. Sci. Eng.: A 753 (2019) 70–78.
[45] M. Tayyebi, B. Eghbali, Microstructure and mechanical properties of SiC-particle-strengthening tri-metal Al/Cu/Ni composite produced by accumulative roll bonding process, Int. J. Miner., Metall. Mater. 25 (3) (2018) 357–364.
[46] M. Kadkhodaee, H. Daneshmanesh, B. Hashemi, J. Moradgholi, Investigation of tribological characteristics of Al/nano SiO2 nanocomposites produced by Accumulative Roll Bonding (ARB) process, Iran. J. Mater. Sci. Eng. 11 (1) (2014) 39–45.
[47] M. Shaat, A. Fathy, A. Wagih, Correlation between grain boundary evolution and mechanical properties of ultrafine-grained metals, Mech. Mater. 143 (2020), 103321.
[48] A. Wagih, M. Shaat, The dependence of accumulative roll bonded copper mechanical properties on grain sub-division, stacking faults, and lattice strains, Mater. Sci. Eng.: A 756 (2019) 190–197.
[49] S. Tamimi, M. Ketabchi, N. Parvin, M. Sanjari, A. Lopes, Accumulative roll bonding of pure copper and IF steel, Int. J. Met. 2014 (2014) *1–9*.
[50] A. Melaibari, A. Fathy, M. Mansouri, M.A. Eltaher, Experimental and numerical investigation on strengthening mechanisms of nanostructured Al-SiC composites, J. Alloy. Compd. 774 (2019) 1123–1132.
[51] M.S. Abd-Elwahed, A. Wagih, I.M.R. Najjar, Correlation between micro/nano-structure, mechanical and tribological properties of copper-zirconia nanocomposites, Ceram. Int. 46 (1) (2020) 56–65.
[52] M.S. Abd-Elwahed, A.F. Meselhy, Experimental investigation on the mechanical, structural and thermal properties of Cu–ZrO2 nanocomposites hybridized by graphene nanoplatelets, Ceram. Int. 46 (7) (2020) 9198–9206.
[53] I.M.R. Najjar, A.M. Sadoun, G.S. Alsoruji, M. Abd Elaziz, A. Wagih, Predicting the mechanical properties of Cu–Al2O3 nanocomposites using machine learning and finite element simulation of indentation experiments, Ceram. Int. 48 (6) (2022) 7748–7758.
[54] A.M. Sadoun, M.M. Mohammed, E.M. Elsayed, A.F. Meselhy, O.A. El-Kady, Effect of nano Al2O3 coated Ag addition on the corrosion resistance and electrochemical behavior of Cu-Al2O3 nanocomposites, J. Mater. Res. Technol. 9 (3) (2020) 4485–4493.
[55] A. Sadoun, A. Ibrahim, A.W. Abdallah, Fabrication and evaluation of tribological properties of Al2O3 coated Ag reinforced copper matrix nanocomposite by mechanical alloying, J. Asian Ceram. Soc. 8 (4) (2020) 1228–1238.
[56] A.M. Sadoun, A.F. Meselhy, A.W. Abdallah, Microstructural, mechanical and wear behavior of electroless assisted silver coated Al2O3–Cu nanocomposites, Mater. Chem. Phys. 266 (2021), 124562.
[57] A.M. Sadoun, I.R. Najjar, G.S. Alsoruji, M.S. Abd-Elwahed, M.A. Elaziz, A. Fathy, Utilization of improved machine learning method based on artificial hummingbird algorithm to predict the tribological behavior of Cu-Al2O3 nanocomposites synthesized by in situ method, Mathematics 10 (8) (2022) 1266.